Neutron Total Cross Sections in the kev Region by Fast Time-of-Flight Measurements

W. M. Good, J. H. Neiler, and J. H. Gibbons
Oak Ridge National Laboratory, Oak Ridge, Tennessee
(Received October 7, 1957)

A new method employing millimicrosecond time measurement has been used to study neutron total cross sections in the 2- to 30-kev energy range. The method has been applied to the nuclides Na^{23}, Al^{27}, P^{31}, K^{39}, K^{41}, Rb^{85}, Rb^{87}, Sr^{86}, Sr^{88}, Y^{89}, Bi^{209}, and to natural Ti, Se, and Pb. A general result is that with the improved resolution of the new instrument, some new levels have appeared and a few previously reported were not observed. Of some special interest is the 2.8-kev resonance in Na^{23} which was definitely shown to have $J=1$, $\sigma_0=380\pm10$ barns. It was observed that the strength function drops about a factor of ten when two protons are added to Rb^{87} to make Y^{89}.

INTRODUCTION

FOR studying the interaction of neutrons with nuclei, neutrons of well-defined energies are required. There are two general methods for obtaining such neutrons. The Van de Graaff electrostatic generator can be used with suitable choice of target and accelerated positive ion to produce neutrons from approximately 1 kev to above 20 Mev in energy. It is not practical to produce specifically monoenergetic neutrons of less than 1-kev energy, so instead it has been the practice to choose such energies from a continuous distribution of energies by means of the time-of-flight technique. When this method is employed, the continuous spectrum of neutrons from which selection is made may either originate in a reactor and be mechanically chopped, or may be generated by moderation of bursts of high-energy neutrons produced by a cyclotron, betatron or linear accelerator. These two methods have had their greatest success, respectively, in the region above about 20 kev and below about 2 kev. This leaves a restricted but important energy range of from about 2 kev to about 20 kev into which the already mentioned techniques can penetrate only with some difficulty.

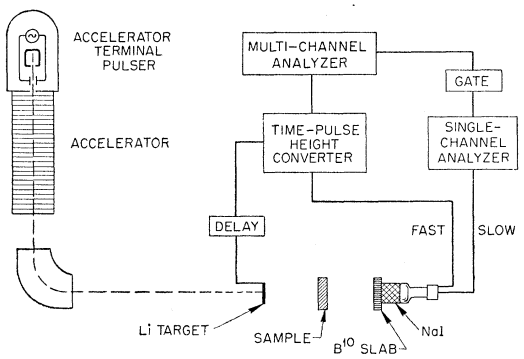

FIG. 1. Block diagram of experimental apparatus. Protons are pulsed in the accelerator terminal by means of an rf sweep across a slit. Neutron bursts are produced at the target by means of the $Li^7(p,n)Be^7$ reaction. Time zero is established by the current pulse on the target. Neutron detection is accomplished by capture in B^{10}. A NaI(Tl) crystal views the 478-kev gamma ray from the $B^{10}(n,\alpha)Li^{7*} \rightarrow Li^7+\gamma$ reaction.

This paper describes results obtained with a technique specifically designed to cover the energy range 2 to 20 kev. The method employs a pre-acceleration pulsed 3-Mv Van de Graaff to produce 5 to 10×10^{-9} sec bursts of neutrons from the $Li^7(p,n)Be^7$ reaction.[1] By suitable choice of target thickness and proton bombarding energy, a spectrum of neutrons is produced at 0° to the proton beam for covering part or all of the kilovolt region to be studied. These *unmoderated* neutrons constitute the source from which energies are chosen by time-of-flight measurements. The technique is therefore a combination of the Van de Graaff and time-of-flight techniques in which the Van de Graaff supplies only the required spectrum of neutrons and the time-of-flight measurement establishes the precise energy.

EXPERIMENTAL TECHNIQUE

A. Instrumentation

The system for production of fast, high-intensity proton pulses, fast detection of the resultant neutrons and multichannel presentation of the time-of-flight data will be described in detail elsewhere.[2] A simplified block diagram is given in Fig. 1.

A proton beam of about 400 μa is deflected past an aperture in the electrostatic generator terminal to produce triangular pulses of about 10 mμsec (width at half maximum) at about 1.3-μsec intervals. The neutron detector is a slab of compacted B^{10},[3] closely backed by a NaI(Tl) scintillation counter. A single channel window is set over the full energy peak of the 480-kev gamma ray from $B^{10}(n,\alpha\gamma)Li^7$. This signal gates into a multichannel pulse-height analyzer the output of a time to pulse-height converter which operates on the time interval between fast signals obtained from the detector and time markers obtained by amplification of the beam pulses on the target.

[1] Neiler, Kelley, and Bell, Bull. Am. Phys. Soc. Ser. II, 1, 70 (1956); V. E. Parker and R. F. King, Bull. Am. Phys. Soc. Ser. II, 1, 70 (1956); Banta, King, and Judish, Bull. Am. Phys. Soc. Ser. II, 1, 70 (1956); Smith, Gibbons, Good, Neiler, and Banta, Bull. Am. Phys. Soc. Ser. II, 1, 71 (1956).

[2] J. H. Neiler *et al.* (to be published).

[3] Prepared by Norton Company, Worcester, Massachusetts. The B^{10} density in this material is 85% theoretical crystal density.

When a 3×3 NaI(Tl) crystal, mounted on a DuMont 6393 photomultiplier is used with a 5-in.×½-in. B^{10} slab the efficiency for detection of the Li^{7*} gamma ray is about 10%. With this detector the over-all time resolution of detector plus time to pulse-height converter is about 6–8 mμsec full width at half maximum.

B. $Li^7(p,n)Be^7$ Reaction as a Source of Unmoderated Neutrons

The important features of the $Li(p,n)$ reaction, so far as the present application is concerned, are (i) the yield with proton energy above neutron threshold, (ii) the dependence of the neutron energy on proton energy, and (iii) the energy dependence of the laboratory angular distribution. The neutron yield has been shown to rise very rapidly at threshold because of a resonance.[4] In the neighborhood of threshold, the neutron energy and angular distribution vary rapidly with proton bombarding energy in a manner derivable from the mechanics of the center-of-mass motion. The equations are:

$$E_n=\frac{M_nM_p}{(M_{\mathrm{Li}}+M_p)^2}\times\left[E_p^{\frac{1}{2}}\cos\theta\pm\left(\frac{M_{\mathrm{Be}^7}M_{\mathrm{Li}^7}}{M_nM_p}(E_p-E_{\mathrm{th}})-E_p\sin^2\theta\right)^{\frac{1}{2}}\right]^2, \quad (1)$$

$$\left|\frac{dN}{d\theta}\right|=\frac{2\pi\sin\theta}{Z}\alpha[\cos\theta\pm Z]^2, \quad (2)$$

$$\left|\frac{dE_n}{d\theta}\right|=2E_p\frac{\sin\theta}{Z}\frac{M_pM_n}{(M_p+M_{\mathrm{Li}^7})^2}[\cos\theta\pm Z]^2, \quad (3)$$

$$\left|\frac{dN}{dE_n}\right|=\frac{dN/d\theta}{dE_E/d\theta}=\pi(M_p+M_{\mathrm{Li}^7})^2\times[M_nM_pM_{\mathrm{Li}^7}M_{\mathrm{Be}^7}E_p(E_p-E_{\mathrm{th}})]^{-\frac{1}{2}}, \quad (4)$$

where

$$\alpha^2=\frac{M_nM_p}{M_{\mathrm{Be}^7}M_{\mathrm{Li}^7}}\frac{E_p}{(E_p-E_{\mathrm{th}})}, \quad Z^2=\left(\frac{1}{\alpha^2}-\sin^2\theta\right).$$

The first equation shows the two-valued character of the neutron energy at each proton energy.[5] At an angle of 0° to the beam the lower branch of neutron energies ranges from 30 kev downwards, and is the group employed for the kilovolt range of neutron energies. Equation (4) shows that near threshold the number of neutrons per energy interval increases as the bombarding energy approaches threshold from above. Equations (2) and (3) show that this increase is the result of a forward concentration of the emitted neutrons as a consequence of center-of-mass motion. This concentration of neutrons into smaller angles as 30 kev is approached is partially compensated by the drop in yield as the bombarding proton energy is lowered toward threshold. It is an observed fact that with targets a few kev thick and a detector subtending about 2° half-angle the number of neutrons per energy interval actually increases approaching 30 kev. Thus, with the accompanying forward "focusing" it is possible to increase the flight path as the energy is increased at no loss of counts per energy interval, and hence to cover the energy range 2 kev to 30 kev with constant fractional energy resolution. Because of the short flight paths employed, it is very easy to keep the flight times of all neutrons approximately constant by varying the distance from target to detector. Figure 2 shows the primary neutron spectrum from targets of two different thicknesses. In this figure the high- and low-energy groups of neutrons are evident. Note that the number of neutrons per unit energy interval for the slowest and fastest neutrons were the same for the two targets. This is predicted by Eq. (4). A smooth, slowly varying neutron spectrum is highly desirable for cross-section studies in order to minimize errors arising from slight spectrum shifts. Thus an ideal spectrum would be one that rises as rapidly as possible at the low-energy end to a plateau, before rising on to the higher energy peak. Curve (b) of Fig. 2 is a good approximation to this type of spectrum.

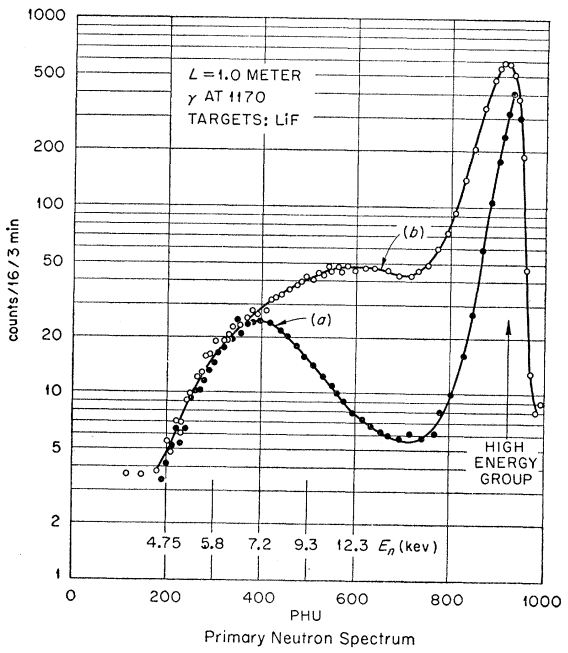

FIG. 2. Neutron yields from two thin lithium targets. The abscissa in pulse-height units (phu) is proportional to neutron momentum. The two 0° neutron energy groups near threshold are evident in the curve (a). Note that the overlap of curves (a) and (b) at the upper and lower energies shows that neutrons per unit energy interval is not increased with target thickness. The only effect of thickening a target is to increase the energy range of neutron production.

[4] R. L. Macklin and J. H. Gibbons, Phys. Rev. **109**, 105 (1958).
[5] Hanson, Taschek, and Williams, Revs. Modern Phys. **21**, 635 (1949).

It seems clear that it is desirable to reduce to a minimum the number of neutrons outside the energy region of interest. Hence, it is the practice to employ targets whose thickness just about corresponds to the maximum energy range desired.

C. Flight Path and Resolution

In order to maintain best resolution as a function of neutron energy, the proton bombarding energy is adjusted to produce a neutron spectrum with a low-energy cutoff immediately below the region of interest. Thus, the flight path can be kept at a maximum and the fractional energy resolution constant. The energy range from 2 to 30 kev has usually been covered with about five flight path positions, ranging from 0.55 to 2.0 meters. A burst repetition rate of about 800 kc/sec has been used. This, of course, is somewhat arbitrary, but has been chosen to permit 1200-mμsec flight times without burst overlap and out of such other considerations as background, counting rate, and sample and detector size. The resolution time itself consists of ion burst duration and filter and electronics time resolution. The over-all time resolution is presently maintained at 12 mμsec.

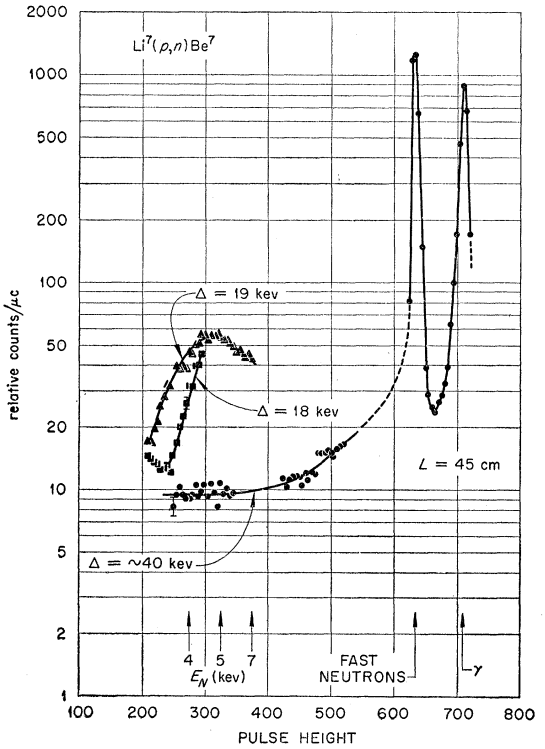

FIG. 3. Sensitivity of neutron spectrum to incident proton energy. The symbol Δ represents the number of kev the proton energy is above the reaction threshold. This fast variation demands unusual requirements upon accelerator energy stability. Transmission samples are rotated from "in" to "out" every few minutes to minimize effects due to primary spectrum changes.

D. Samples

The transmission samples that were used in the results to be presented were $\frac{1}{2}$-inch diameter cylinders, canned in thin-walled silver cups for protection. For average sample thicknesses, about 0.05 mole of material were needed. The use of somewhat smaller samples should be quite feasible but would require a more careful alignment method than so far used. Samples were used either in elemental form or as oxides or fluorides. The enriched isotopes used were obtained on loan from the Oak Ridge National Laboratory Isotopes Division.

E. Targets

Both Li^7 metal and Li^7F vacuum evaporated targets have been used. Li^7F targets can be stored with ease since they are chemically inactive. Li^7 metal targets are stored and transferred in inert gas. Although the Li^7 metal targets initially produced more neutrons per unit energy interval than those of LiF, a slow deterioration of the Li^7 metal targets has been observed resulting in noticeable shifts in the neutron spectrum over a period of a day. This has been attributed to the building up of surface layer contaminants, principally due to the high reactivity of the lithium metal. An analysis of neutron groups emerging from bombardment of "lithium metal" targets with deuterons indicated the presence of appreciable quantities of both carbon and oxygen.

Since target stability is essential we decided to use Li^7F targets. No appreciable deterioration has been noted under the same conditions as described for the metal targets.

The spectrum change for slight changes of target condition (or incident proton energy) is demonstrated in Fig. 3. A change in bombarding energy of only one kev caused a significant change in the neutron spectrum. For this reason transmission samples were rotated from "in" to "out" every few minutes in order to cancel any slow changes in the spectrum. The counts were stored in two separate 20-channel analyzers and read out only after sufficient counting statistics had been obtained.

Standardization of counts was accomplished both by proton current integration and neutron flux monitoring.

F. Background

(1) The principal source of background in the detector so far has been "room" radiation, principally from natural sources, other accelerators and reactors. Unfortunately, most attempts at reducing this background by local shielding have resulted in sufficient neutron in-scattering to cause a distortion of observed spectrum shape. The reason is fast singly scattered neutrons that arrive at the detector simultaneously with slower, direct neutrons will be assigned the wrong energy. Many of the data presented in this paper were taken using a completely unshielded detector. During

TABLE I. Comparison of time-of-flight and back-angle Van de Graaff techniques for measuring kev neutron cross sections.

	1 Max beam on target	2 Av beam	3 Neutrons ΔE	4 ΔE_n at 10 kv	5 Neutrons/ background at 10 kv	6 Time 1000 counts×100 ev	7 No. of channels	8 Principal source of background	9 Half-angle at detector	10 Target thickness	11 Minimum moles needed for 1×10^{22} atoms/cm²
Time-of-flight	400 μa	1.25 μa	Comparable	200 ev	~10/1	18 min	20	Room γ's	½° to 2°	4000 ev	0.05
Van de Graaff	40 μa	40 μa	Comparable	300 ev	~10/1	2.5	1	Scattered neutrons	⅕°	300 ev	≫0.05

more recent runs, a specially designed 5-in. o.d. lead shield was used over a 3 in.×3 in. NaI crystal. The 5-in. diameter B^{10} slab was mounted on this system to complete the detector. The B^{10} slab shielded both lead and NaI from the lower energy neutron group. Fast neutrons in-scattered by the lead had only slightly longer flight times than did the direct fast neutron beam. In this manner the "room" background can be reduced by about 30% without noticeable spectrum distortions.

(2) No increase in background is noted with beam on target when proton energy is less than threshold. Pulse leakage current has been found to be less than 10^{-3}% of the pulse peak current.

(3) The increase (other than detector activation) in background for $E_p > E_{\text{th}}$ was found to be only several percent of the "room" background. This component is due to air and floor scattered neutrons.

(4) Some neutrons penetrate the B^{10} slab and are captured by iodine in the NaI detector. These induce a background due to that portion of the I^{128} beta spectrum that falls in the "window" set to view $B^{10}(n,\alpha\gamma)$ captures. The variation of this 25-min activity in practice has been reduced by running the equipment for about an hour before taking data.

Average relative contributions from the effects mentioned above are, respectively, 12:0:2:4. The approximate total background for maximum flight paths varies from 30% at 2 kev to 10% at 10 kev. The average data taking time required to obtain a transmission with 2.5% counting statistics over the energy range from 3 to 30 kev is about 20 hours.

G. Evaluation

The approach that has just been described to measure neutron total cross sections in the kilovolt region differs in so many respects from the standard chopper and back angle Van de Graaff techniques that it was initially uncertain whether the advantages the new technique appeared to possess might in fact be more than compensated by the attendant difficulties. Table I gives a comparison between the back-angle Van de Graaff method and the present method.

Although the average pulsed beam in the time-of-flight method is considerably smaller than the average steady beam of the back-angle method, the times for covering a given energy range are comparable. The fact that the two methods are so different may make this conclusion somewhat surprising, but the reasons are as follows: precise energy control of the unpulsed Van de Graaff together with target limitations makes 40 μa of average steady beam a very generous figure for the average current that might be used in the standard back angle technique. At the same time this standard technique takes data, energy interval by energy interval. In these two respects the time-of-flight technique is entirely different from the standard back-angle technique.

By using the time-of-flight method, a peak current on the target of about 400 μa is achieved, the average current being reduced to less than 2 μa by the 0.5% duty as a result of the pulsing. Thus, the pulsed peak current that can be used is at least ten times the steady current that can be used. Finally, the time-of-flight method simultaneously measures a range of energies and this range covers about ten settings of the Van de Graaff in the standard method.

The resolution figures in Table I require some comment. First, generous allowances have been made in estimating the best the standard Van de Graaff technique can do. On the other hand, the resolution figure quoted for the time-of-flight method is what the present instrument has been designed to achieve, and further improvement seems possible. Second, the resolution figures of Table I have to be weighed by the relative ease with which the electronics of the time-of-flight method can be maintained as compared with the ease with which targets of 300 ev equivalent thickness can be maintained clean and uniform, and the electrostatic generator voltage held steady within 200 volts. Only experience can decide.

RESULTS AND ANALYSIS

The data presented in this section were obtained at various stages during the development of the technique. Hence, some elements were examined with better resolution than others. Figures 4–9 are representative of the results obtained. A summary of all results so far obtained is given in Table II. Samples were used in elemental form in some cases (Na, Al, P, Ti, Y, Pb, and Bi) and as oxides or fluorides in the remaining cases. Correction for the fluorine or oxygen cross section was made assuming $\sigma(\text{F})=3.7$ barns and $\sigma(\text{O})=3.8$ barns.

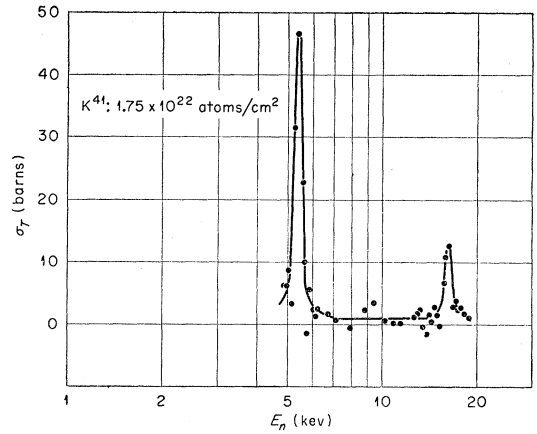

FIG. 4. Total cross section of K^{41} as a function of energy.

With few exceptions natural widths of resonances studied were less than the experimental resolution. Under these conditions the most convenient technique for determining true resonance widths from experimental transmissions is that of *area analysis*,[6–8] in which the true width can be extracted from the area of the transmission dip due to the resonance.

If a resonance is isolated so that the full area of the transmission dip can be measured, the area has a simple relationship to the width for extremes of sample thickness.[8] However, in practice the total area is often difficult to obtain, usually because of closely neighboring resonances. In this case it is convenient to limit the area integration to an energy interval, 2ϵ, located symmetrically about the resonance peak at E_0, where one chooses $2\epsilon \gg \Gamma$. Then the area above the transmission dip between energy limits $(E_0-\epsilon)$ and $(E_0+\epsilon)$ is related to a calculable function $Z(2\epsilon/\Gamma, n\sigma_0)$.[6] The width is then extracted from this relation.

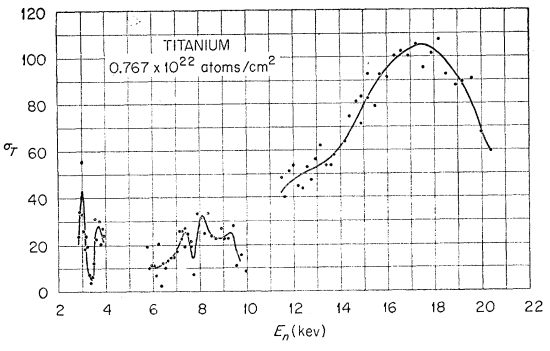

FIG. 5. Total cross section of natural titanium as a function of energy. The peak at 17.5 kev, due to Ti^{48}, is about 7 kev wide but may be complex. These results clearly indicate the need for investigation with separated isotopes.

[6] E. Merzbacher, "Analysis of neutron transmission experiments" (unpublished).
[7] Melkonian, Havens, and Rainwater, Phys. Rev. **92**, 702 (1953).
[8] Seidl, Hughes, Palevsky, Levin, Kato, and Sjostrand, Phys. Rev. **95**, 476 (1954).

Note that a knowledge of σ_0 is presumed if a unique value of Γ is to be determined from a measurement on a single sample thickness. Since (in the kev range) nuclei with level spacings of the order of 100 ev or more have $\Gamma_n \approx \Gamma_{\text{total}}$, one can calculate σ_0/g from a knowledge of E_0. This is sufficient to determine σ_0 for nuclei of spin $I=0$ or $I \gg 1$, but not for $I \sim 1$. With the exception of sodium, yttrium, and titanium the results (Table II) were obtained for single sample thicknesses only. We have made the approximation in calculating these widths that for $I \neq 0$, $g=\frac{1}{2}$.

DISCUSSION

Na^{23}

The low-energy resonance in sodium has received a great amount of attention in the past decade[9–14] because of its unusual width and shape as well as its importance in the field of reactor technology. Selove[9] interpreted the results of Hibdon *et al.*[10] with an assigment of $J=2$, $l=0$. He assumed a spin-dependent potential scattering to account for the absence of an interference dip in the total cross section. An alternative suggestion by Stelson and Preston[11] and also Toller and Newson[12] was that the resonance might be due to p-wave neutrons. Later chopper work[13] again reported $J=2$. However, in a recent report from Harwell by

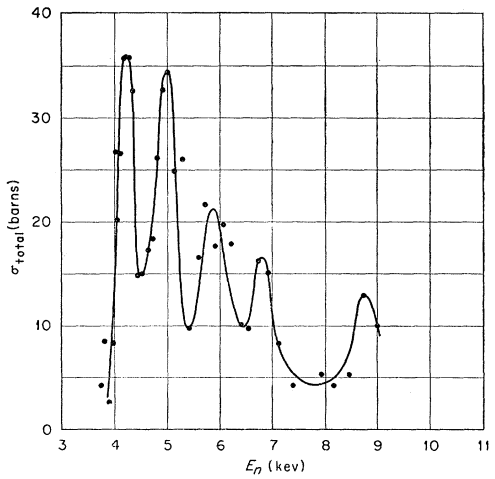

FIG. 6. Total cross section of natural selenium as a function of energy. Previous data had indicated only a single, broad maximum in this region.

[9] W. Selove, Phys. Rev. **80**, 290 (1950).
[10] Hibdon, Muehlhause, Selove, and Woolf, Phys. Rev. **77**, 730 (1950).
[11] P. H. Stelson and W. M. Preston, Phys. Rev. **88**, 1354 (1952).
[12] A. L. Toller and H. W. Newson, Phys. Rev. **99**, 1625 (1955).
[13] *Neutron Cross Sections*, compiled by D. J. Hughes and J. A. Harvey, Brookhaven National Laboratory Report BNL-325 (Superintendent of Documents, U. S. Government Printing Office, Washington, D. C., 1955) (unpublished data of Brookhaven Fast Chopper Group).
[14] Lynn, Firk, and Moxon, Harwell Report TNCC(UK) **18**, May 20, 1957 (unpublished).

Lynn, Firk, and Moxon,[14] a new measurement was reported which was made on the linear accelerator time-of-flight spectrometer. The results were interpreted as showing $J=1, l=0$.

In view of the conflicting results, the cross sections near 3 kev were measured with the present instrument by employing very thin metallic samples ranging from 0.11×10^{22} to 6.4×10^{22} atoms/cm^2. The results gave values for the cross sections that were in good agreement with the Harwell results in the entire energy range common to both sets of measurements.

With the peak cross section fixed at 380 ± 10 barns, it is certain that $J=1$. On the other hand, an assumption of either $l=0$ or $l=1$ gives a respectable fit to the cross section as a whole. There are two reasons at present for preferring $l=0$. In the first place, a better fit to all the data can be obtained assuming $l=0$ together with a contribution from a $J=2$ level at negative neutron energy than can be obtained assuming $l=1$. In

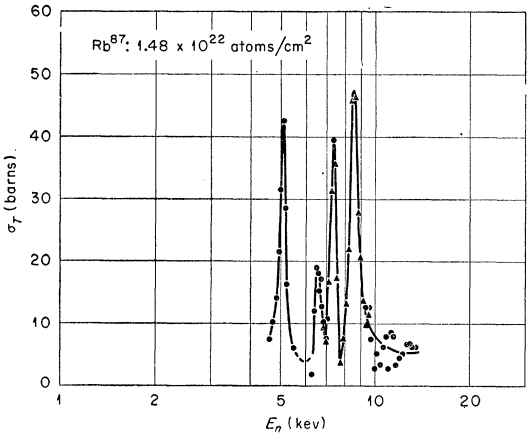

FIG. 7. Total cross section of Rb^{87} as a function of energy.

the second place, a large value for the reduced width accompanies the assumption of $l=1$, for any reasonable value of the nuclear radius, so it would seem that $J=1, l=0$. However, it should be added that in spite of the arguments in favor of $l=0$, the cloudy crystal-ball model does predict a $2p$ giant resonance near $A=25$. Hence, somewhat stronger proof seems desirable to eliminate completely the possibility $l=1$.

Al

Rohrer *et al.*[15] reported a resonance near 6 kev in a study of the activation $Al^{27}(n,\gamma)Al^{28}$. This resonance is principally responsible for the activation cross section below 10 kev. Its radiation width was estimated to be 1.5 ev. The result of the total cross-section measurement, $\Gamma=20$ ev, indicates a ratio $\Gamma_\gamma/\Gamma_n\sim0.1$.

[15] Rohrer, Newson, Gibbons, and Cap, Phys. Rev. **95**, 302(A) (1954).

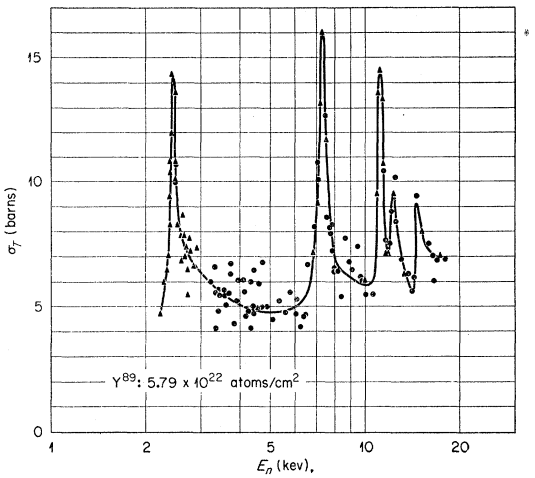

FIG. 8. Total cross section of Y^{89} as a function of energy. In contrast to the results for Rb^{85} and Rb^{87}, this nuclide exhibits rather narrow resonance widths.

K^{39}, K^{41}

An earlier study[16] of potassium indicated several peaks below 30 kev, including resonances in both isotopes near 10 kev. We were unable to observe any peak in K^{41} between 5.4 and 16.2 kev but did observe a resonance at 9.2 kev in K^{39}. The cross-section behavior of these two isotopes appears to be quite similar both in level density and strength function. The values listed in Table II for the strength function were derived both from our measurements and the results of Toller *et al.*[16] at higher energies.

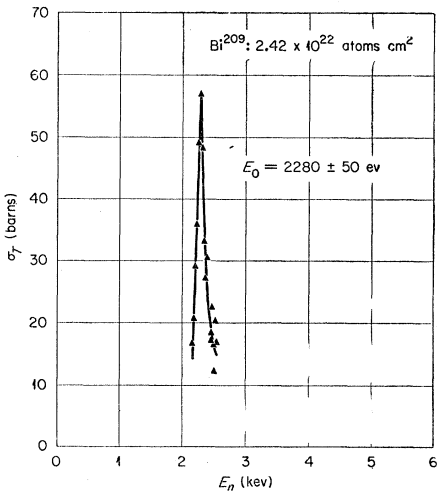

FIG. 9. A resonance in the total cross section of bismuth. This relatively well-known level has been studied with several techniques. Because of its small natural width (about 20 ev), it provides a convenient test for instrumental resolution.

[16] Toller, Patterson, and Newson, Phys. Rev. **99**, 620(A) (1955).

TABLE II. Summary of kev neutron cross-section measurements.

Nuclide	Atoms $10^{-22}\times$No. atoms/cm^2	Isotopic purity	Energy interval studied (kev)	E_0 (kev)(Γ(ev))	D_{obs} (kev)	$\bar{(\Gamma_n^0/D_0)}\times10^4$	Remarks
Na^{23}	6.41, 0.265, 0.11	(100)	2.4– 8	2.80(420, $l=0$, 370, $l=1$)	···	···	$J=1$, $\sigma_0=380\pm10$ b
Al^{27}	7.65	(100)	5 – 6.2	5.6(20)	···	···	l probably >0
P^{31}	6.10	(100)	6 –20	···	···	···	σ decreases smoothly from 5.0 b at 8 kev to 4.0 b at 20 kev
K^{39}	2.27	99.7	3 –10	3.4(12), 9.2(60)	10	0.9	
K^{41}	1.75	98.3	5 –20	5.4(35), 16.2(60)	10	1.0	
Ti	3.65, 0.767	Natural	3 –20	3.0(50), 3.7, ···, 17.5(7000)	···	···	Resonance at 17.5 kev and probably the one at 3.0 kev are due to Ti^{48}
Se	1.19	Natural	3.8– 9	4.25(35), 4.95(35), 5.85, 6.8, 8.6	···	···	Width assignments assumed s-wave neutrons on Se^{80}
Rb^{85}	2.04	99.1	3 – 9	3.3, 4.1(18), 4.9(34), 5.8(33), 6.9(17), 9?	1.0	1.8	$N=48$
Rb^{87}	1.48	94.9	4.5–15	5.0(46), 6.6(17), 7.35(54), 8.55(170)	1.7	2.4	$N=50$
Sr^{86}	1.50	88.6	3 –15	3.0, 4.3, 11.3	4	···	$N=48$
Sr^{88}	2.09	99.6	7 –20	13.6(400)	15	···	$N=50$
Y^{89}	5.79, 1.93	(100)	2.2–18	2.5(6), 7.35(55), 11.25(60), 14, 17	3.0	0.25	$N=50$
Pb	10.48	Natural	20 –34	···	···	···	No fluctuations $>10\%$ of $\sigma_{pot}(=10.2$ b) were observed
Bi	2.42	(100)	2.2– 2.6	2.3(24), 12.5, 15.5, 33	7	···	D_{obs} includes resonance at 0.8 kev

Ti

Previous studies of the total cross section of natural titanium have been made with both chopper[17] and Van de Graaff[18] techniques. These studies indicated small resonance effects near 3 kev as well as an unusually large peak near 18 kev. Our results show that the cross section is complex, presumably due to resonance contributions from several isotopes. The peak at 17.5 kev is principally due to Ti^{48} and appears to be about 7 kev wide. Assuming the peak is due to a single s-wave resonance the reduced width is about 1% of the Wigner single particle limit. The maximum reported near 3 kev is clearly due to at least two resonances. The peak at 3.0 kev is probably due to Ti^{48} and, if so, has a width of 50 ev. This element will be re-examined by using enriched isotopes.

Se

To indicate the improvement experienced in resolution, the five peaks found in this energy interval were only recently reported as a single broad maximum.[19,20] Bollinger[21] has also observed that several peaks exist in this region. Similarly to the case of Ti, any further work on this element will have to be done with enriched isotopes.

$Rb^{85,87}$, $Sr^{86,88}$, and Y^{89}

The region $A=80$–100 is of considerable interest for several reasons. First, the magic neutron number $N=50$ occurs in this region. Secondly, in this region a strangely deep minimum in the s-wave strength function, $\bar{\Gamma}_n^0/D$, has been reported.[22] Also one expects around $A=100$ the $3p$ giant resonance. We have chosen, wherever possible, isotopic pairs (differing by 2 identical nucleons) such as the isotopes Rb and Sr so that one may study the spacing and other parameters as a shell is filled with as few extraneous circumstances as possible. The data collected thus far are admittedly far from a good statistical average, but certain effects are already quite evident. First, especially for the case of $Sr^{86,88}$ one sees a marked increase in level spacing as the shell is closed. However, the change in spacing from Rb^{85} to Rb^{87} is surprisingly small. Secondly, the strength functions for Rb^{85} and Rb^{87} are equal, within statistics. Finally, one sees a rather dramatic effect when two protons are added to Rb^{87}, forming Y^{89} in that the strength function is dramatically decreased. The effect appears to be roughly an order of magnitude. The possibility that some of the levels observed are due to p-wave neutrons certainly exists and could conceivably complicate any interpretation. However, for energies as low as 10 kev the high p-wave centrifugal barrier is certainly a strong inhibitor of such an effect.

ACKNOWLEDGMENTS

The authors wish to make special acknowledgment of the contribution of E. C. Smith to whom credit is

[17] *Neutron Cross Sections*, compiled by D. J. Hughes and J. A. Harvey, Brookhaven National Laboratory Report BNL-325 (Superintendent of Documents, U. S. Government Printing Office, Washington, D. C., 1955) (unpublished data from Argonne Fast Chopper Group).

[18] *Neutron Cross Sections*, compiled by D. J. Hughes and J. A. Harvey, Brookhaven National Laboratory Report BNL-325 (Superintendent of Documents, U. S. Government Printing Office, Washington, D. C., 1955) (unpublished data from Argonne Electrostatic Accelerator Group).

[19] Bollinger, Dahlberg, Palmer, and Thomas, Phys. Rev. **100**, 126 (1955).

[20] Newson, Gibbons, Marshak, Williamson, Mobley, Toller, and Block, Phys. Rev. **102**, 1580 (1956).

[21] L. W. Bollinger (private communication).

[22] V. F. Weisskopf, Revs. Modern Phys. **29**, 174 (1957).

due for many original ideas and as a partner in some of the first measurements. It is also a pleasure to recognize valuable contributions to the instrumental development from C. D. Moak, R. F. King, V. E. Parker, H. E. Banta, and C. H. Johnson. Helpful discussions with H. W. Newson and J. A. Harvey are gratefully acknowledged. R. C. Block and R. L. Macklin were active collaborators in the sodium measurement. The measurements on separated isotopes were made possible by the cooperation of P. S. Baker and his collaborators of the Oak Ridge National Laboratories Stable Isotopes Division.

PHYSICAL REVIEW VOLUME 109, NUMBER 3 FEBRUARY 1, 1958

Velocity-Dependent Forces and Nuclear Structure. II. Spin-Dependent Forces

MARCOS MOSHINSKY
Instituto de Física, Universidad de México e Instituto Nacional de la Investigación Científica, Mexico, D.F., Mexico
(Received May 6, 1957; revised manuscript received August 5, 1957)

Recent investigations have shown the presence of velocity-dependent forces in the two-nucleon interaction, increasing the number of parameters in the two-nucleon potential, and making more difficult the determination of these parameters in a unique way. In view of the successes of the shell model and of the assumptions that the same interactions hold between nucleons inside nuclear matter as between free nucleons, it is of interest to explore the possible restrictions on the two-nucleon potential that follow from level arrangements and separations in nuclear shell theory. In the present paper we carry out this exploration for velocity-dependent forces, starting with the two-body spin-orbit force, two forms of which have recently been proposed, and considering also the simplest velocity-dependent forces that depend on the second power of the momentum, which include the velocity-dependent tensor force recently introduced by Breit. The two-body spin-orbit force of Gammel and Thaler has a very short range, and, taking advantage of this fact, we show in Sec. 2 that the interaction energy for two nucleons in the same shell is proportional to the interaction energy for the zero-range velocity-dependent central force discussed previously by the author. The simple expression for the interaction energy allows us to compare in Sec. 3 the level separation due to the spin-orbit force of Gammel and Thaler and that due to the spin-orbit force of Signell and Marshak. We also compare the effects of both types of spin-orbit forces with the interaction energy due to the central even singlet force of Gammel, Christian, and Thaler. In Sec. 4 we analyze a velocity-dependent central force that acts only in the triplet state. In Sec. 5 we discuss the velocity-dependent tensor potential in the long-range approximation, and show the restrictions that follow on the strength of this potential from the assumption that the separation between levels should be small compared with the separation between shells. In Sec. 6 we discuss the velocity-dependent tensor potential in the short-range approximation, and obtain restrictions on the product of strength and range of this potential. The interaction energies for all short-range velocity-dependent potentials show similarities, suggesting the possibility of finding simple closed expressions for the interaction energies for all short-range forces.

1. INTRODUCTION

IN recent publications it has become clear that velocity-dependent forces play an important role in the interactions between nucleons. In particular, the work of Signell and Marshak[1] and of Gammel and Thaler[2] has shown that the experimental data on the two-nucleon interaction require for its explanation potentials that contain, besides ordinary forces (both central and tensor), a strong spin-orbit coupling force.

The work of Brueckner,[3] Bethe,[4] and their collaborators has shown that it is possible to assume for the interaction between nucleons inside nuclear matter the same potentials as between free nucleons. It is therefore of interest to see the effect of velocity-dependent forces between nucleons on nuclear structure, and particularly on nuclear shell theory. For the two-particle spin-orbit coupling force a general discussion has been given by Hope and Longdon[5] and by Hope.[6] The results of Hope and Longdon are rather complex, as they wanted them to apply to a spin-orbit force whose range was arbitrary. The analysis of Gammel and Thaler[2] shows, however, that the spin-orbit force has a very short range. This property permits a considerable simplification in the analysis, and we shall show that the effects of a short-range spin-orbit force in nuclear shell theory, are similar to those of the short-range velocity-dependent central force discussed by the author in a previous paper[7] (to be referred to as I). The explicit expressions for the interaction energy could be useful to discriminate between the different forms[1,2] of the spin-orbit coupling forces being proposed, particularly as it is possible to take now into account[8] the repulsive hard core present in the force introduced by Gammel and Thaler.[2]

It is well known that the only interaction between like nucleons that satisfies the invariance requirements[9] and depends on the first power of the momentum, is the spin-orbit coupling force. If a further dependence on the velocity is found for the interactions between

[1] P. S. Signell and R. E. Marshak, Phys. Rev. **106**, 832 (1957).
[2] J. L. Gammel and R. M. Thaler, Phys. Rev. **107**, 291 (1957).
[3] K. A. Brueckner, Phys. Rev. **97**, 1353 (1955).
[4] H. A. Bethe, Phys. Rev. **103**, 1353 (1956).
[5] J. Hope and L. W. Longdon, Phys. Rev. **102**, 1124 (1956).
[6] J. Hope, Phys. Rev. **106**, 771 (1957).
[7] M. Moshinsky, Phys. Rev. **106**, 117 (1957), to be referred to as I.
[8] M. Bauer and M. Moshinsky, Nuclear Phys. **4**, 615 (1957).
[9] L. Rosenfeld, *Nuclear Forces* (North-Holland Publishing Company, Amsterdam, 1948), p. 313.